Gochlear implants from model to patients

Briaire, J.J.

Chapter 8

Unraveling the Electrically Evoked Compound Action Potential

Jeroen J. Briaire and Johan H.M. Frijns
Hearing Research (2005), 205(1-2), 143-156

Abstract

With the advent of eCAP recording tools such as NRT and NRI for cochlear implants, neural monitoring has become widely used to ascertain the integrity of the neural/electrode interface as well as for assisting in the setting of program levels. The basic concepts of eCAP recordings are deduced from the acoustical equivalent of the electrocochleogram. There are, however, indications that under electrical stimulation some of these do not hold, like the unitary response concept (i.e., the principle that every fiber produces the same contribution to the eCAP). Computer modeling has proven to be a valuable tool for gaining insight into the functioning of electrical stimulation. In this study the extension of a three-dimensional human cochlea, incorporating back-measuring capabilities, is described. Using this new model, the contribution of single fiber action potentials (SFAPs) to the measured eCAP is investigated. The model predicts that contrary to common belief- the compound action potential as measured by the cochlear implant system does not necessarily reflect the propagated action potential along the auditory nerve.

8.1 Introduction

The recording of electrically evoked compound action potentials (eCAPs) of the auditory nerve has become widespread since the introduction of Neural Response Telemetry (NRT) by Cochlear Ltd. (Sydney, Australia) and Neural Response Imaging (NRI) by the Advanced Bionics corporation (Sylmar, CA, USA). These systems allow easy acquisition of the eCAP through the cochlear implant system without the need of extra recording or stimulating electrodes such as a trans-tympanic needle. The fundamentals of auditory CAP recordings are known from the acoustically evoked equivalent, which is the electrocochleogram. The latter is used in clinical practice as a reliable way to measure a frequency specific objective audiogram (Schoonhoven et al., 1996; Schoonhoven et al., 1999). Stimuli with alternating polarity are used in such acoustically evoked recordings to remove the cochlear microphonic (CM), which results from outer hair cell responses. One of the mainstays of these recordings is that the CAP response can be described as a superposition of unitary responses, meaning that each nerve fiber contributes equally to the signal (Versnel et al., 1992; Goldstein and Kiang, 1958), and that the amplitude of the recorded fiber response correlates with the number of excited nerve fibers. The recording of eCAPs gives rise to some specific issues compared to the electrocochleogram, e.g., now the electrical artifact has to be suppressed instead of the CM. The question that remains is whether all the other principles of acoustical CAP recordings are applicable for eCAP recordings. Moreover, to date the clinical value of using eCAP input/output functions and thresholds to set processor parameters remains limited to finding contours for the levels in the programs. These objective data have to be supplemented by behavioral data to get functional programs (Abbas et al., 1999; Seyle and Brown, 2002; Smoorenburg et al., 2002). It remains unclear, however, what the fundamental problems are why it is not possible to build programs that patients prefer based only on eCAPs. Additionally, the ability to measure refractory properties (Miller et al., 2000) and the possibility to obtain objective measures of spatial selectivity (Cohen et al., 2003; Abbas and Brown, 2000; Frijns et al., 2002) are not yet sufficiently validated in terms of their clinical applicability. More specific questions that need to be answered are, to what extent these objective measures are applicable to the fitting of children or can be used to assess neural degeneration in regions of the cochlea.

To gain further insight into the working mechanisms of electrical stimulation of the auditory nerve by a cochlear implant, a detailed computer model of the cochlea has been developed at the Leiden University Medical Center (Frijns et

al., 2000a; Briaire and Frijns, 2000a). The model consists of two parts, a 3D volume conduction model and an active auditory nerve fiber model. The volume conduction part provides insight into the distribution of the current through the cochlea (Briaire and Frijns, 2000b) and how this distribution can be influenced by, for example, electrode orientation. In and of itself however, the potential distribution does not tell which fibers will react and how the stimulus waveform affects the response. For this purpose the nerve fiber model is used. Using the potential distribution along the nerve fibers for its input, this model calculates which fibers and what part of these fibers will be excited (Frijns and ten Kate, 1994; Frijns et al., 1995). Initially, both models were based upon the cochlea of a guinea pig, our experimental animal, with corresponding fiber morphology and nodal kinetics. The presence of cross-turn stimulation, the unintended and unwanted activation of nerve fibers from a higher turn than where the stimulating electrode is located, and the influence of the electrode position were the main outcomes of this initial model (Frijns et al., 1995; Frijns et al., 1996a). To generate an applicable human model, the animal volume conduction model was extended to use realistic electrode geometries and to match the human cochlear anatomy. This also gave us a tool to investigate the validity of transferring results obtained from animal experiments to the human situation (Frijns et al., 2001). Recently, one of the main outcomes of this study, a decrease in threshold and an increase in neural excitation at a fixed current level when the electrode is moved to a more peri-modiolar position, was confirmed with intra-operative electrically evoked auditory brainstem response (EABR) measurements with the HiFocus electrode in lateral and medial positions by Firszt et al. (2003).

Previous studies, with integrated use of neural and volume conduction models from a number of groups (Hanekom, 2001; Rattay et al., 2001a), typically focused on the so-called forward problem, i.e., predicting the neural excitation pattern. To our knowledge, the first attempt to simulate eCAPs was a preliminary study with a guinea pig model that was in itself just capable of solving the forward problem (Frijns et al., 1996b). It used the assumption that the unitary response concept was also valid for the electrically stimulated cochlea and led to the conclusion that just the site of excitation along the auditory nerve fiber cannot account for the latency differences observed. To answer more subtle questions about the value and possibilities of eCAP recordings and the validity of the unitary response concept a more sophisticated model is needed, which is able to solve the full backward problem, i.e., the calculation of the eCAP response as recorded via intra-cochlear electrode contacts.

As stated above, the geometry of the cochlea and the implant used in our

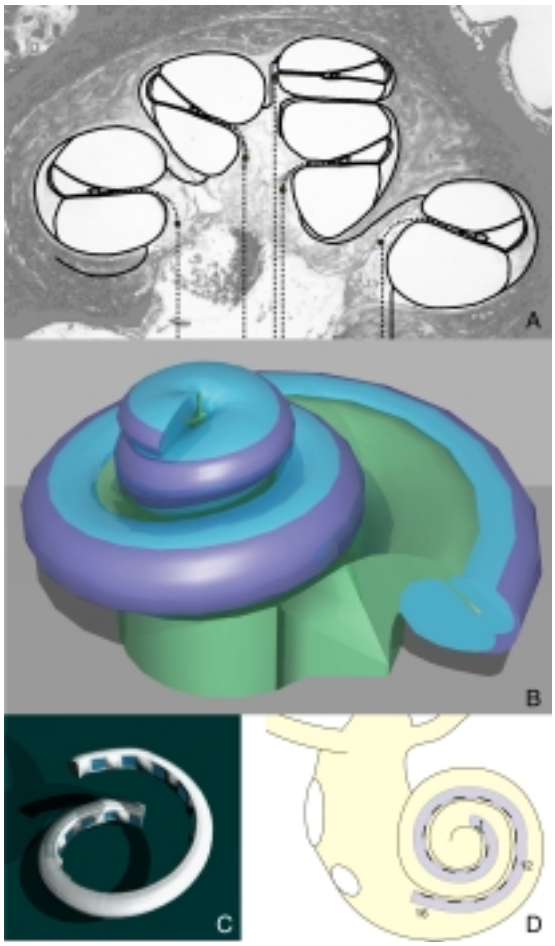

*Figure 8.1: (**A**) Mid-modiolar cross-section of the human cochlea with the cross-section of the volume conduction model shown in bold lines. In the modiolar part of the cochlea the positions of the nerve fibers have been plotted (dotted lines) as well as the approximate locations of the cell-bodies within the spiral ganglion(indicated by solid circles). (**B**) A three-dimensional representation of the cochlear model. (**C**) Model representation of the HiFocus electrode array as used for the simulations. (**D**) Schematic representation of the electrode array in the cochlea, with contacts 1, 12 and 16 numbered.*

previous studies were already in line with the human anatomy. However, the kinetics and morphology of the nerve fibers were still based on the guinea pig, which likely compromised the applicability of the findings to humans. The main anatomical difference between the guinea pig and human primary auditory nerve fiber is the morphology of its cell body, which is unmyelinated in humans as contrasted with all other mammals. From Rattay's model study (Rattay et al., 2001b) it is known that the unmyelinated cell body in the human fiber is likely to play an important functional role, as it induces a delay in the conduction of the action potential (AP) along the fiber. Also the length of the peripheral process in humans is much longer than in guinea pigs. Therefore, there are presumably more than three (the value used in the guinea pig models) inter-nodal segments in the human peripheral process, although there is no formal histological evidence available.

The present study aims at deriving a fundamental understanding of the processes underlying eCAP recordings in humans, both in terms of the contributions of the individual nerve fibers to the overall signal as well as to what extent this signal yields clinically relevant information about functional aspects of electrical stimulation. For this purpose the neural model has been extended to incorporate an unmyelinated cell body and an unmyelinated pre-somatic region. In addition, the algorithms of the volume conduction model have been upgraded to calculate the eCAP from single fiber responses in order to generate simulated wave forms that can be compared with actual recordings.

8.2 Materials and methods

8.2.1 The forward problem: simulating neural excitation in the human cochlea

The computational model of the electrically stimulated human cochlea as described in Frijns et al. (2001) forms the basis of the computational model used in the present study. The model geometry is a realistic three-dimensional representation of the human cochlea with a model representation of the Clarion HiFocus cochlear implant (Fig. 8.1^{A,B,C}). Details of this geometry have been published in the aforementioned paper. Unless stated otherwise, the implant array is in a peri-modiolar position in the scala tympani throughout the present study, as it is expected to be clinically when a peri-modiolar electrode array is used (Fig. 8.1^{D}). The nerve fibers are located in the modiolus and radiate

out into the osseous spiral lamina, with the tips of their peripheral processes evenly distributed below the organ of Corti with a spacing of 100μm. This leads to a total of 299 modeled fibers in the entire cochlea. Each fiber in the model represents a group of 100 actual nerve fibers, limiting the amount of computational effort while preserving sufficient spatial resolution. All simulations in this study are performed with biphasic current pulses with a phase duration of 37.5μs on contact 12 of the array, approximately in the middle of the basal turn. The most apical contact #1, with an insertion of approximately 1.5 turns, is used as recording contact. This situation will be referred to as 'standard conditions'.

As explained in section 8.1, the model consists of two sub-models: First, the volume conduction step calculates the potential distribution and the current spread through the various tissues incorporated in the cochlea model (Briaire and Frijns, 2000a; Briaire and Frijns, 2000b) as a result of the current injected through a stimulated electrode. Thereby, the (quasi-static) volume conduction model calculates the potential $V_{f,k}^{stim}$ on every node of Ranvier k of each fiber f induced by a unit current from the stimulating electrode $stim$, yielding the resistance matrix R^{stim} with elements $R_{f,k}^{stim}$. This matrix serves as the transfer function between the stimulating electrode and the nodes of Ranvier. Then Ohm's law yields the time-varying potential $V_{f,k}^{stim}(t)$ due to a time-varying current stimulus $I(t)$, injected from the stimulating electrode:

$$V_{f,k}^{stim}(t) = R_{f,k}^{stim} I(t) \tag{8.1}$$

The second sub-model is an active, non-linear nerve fiber model, which calculates the neural response elicited by the stimulus. Compared to our previous studies the morphology has been upgraded to get a better representation of the human nerve fiber. Fig. 8.2 shows the fiber morphology as used in this study. It represents a bipolar high spontaneous rate (HSR) nerve fiber with a uniform axon diameter of 3 μm, an inter-nodal length varying between 50 and 350 μm and a nodal gap width of 1 μm. As contrasted to our previous studies, the fiber model now includes a 10 μm thick, cell body (CB) preceded by a thin (axon diameter 2 μm) pre-somatic compartment as initially used by Rattay et al. (2001b). These two segments have been modeled as unmyelinated segments in the so-called unmyelinated cell body (UMCB) condition. In this condition the fiber morphology is in accordance with known human data (Nadol, 1988). The importance of these changes to the modeled fiber morphology was reported by Rattay et al. (2001b), who showed the influence

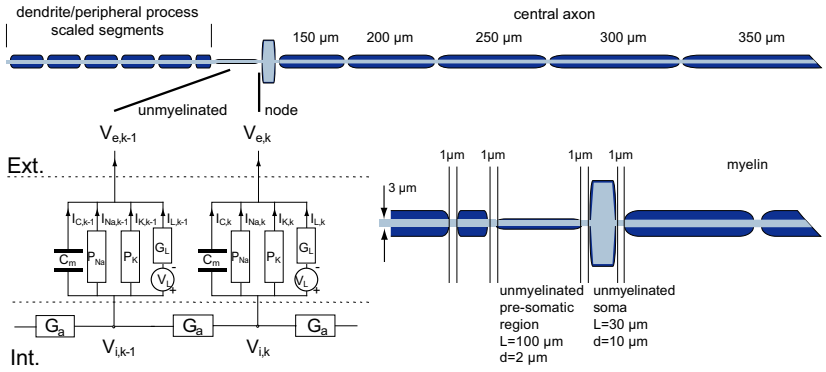

Figure 8.2: Representation of the nerve fiber morphology. The peripheral process consists of 6 scalable segments to adjust for the variable length from the organ of Corti to the cell body. In the UMCB condition the pre-somatic region and the cell body were modeled as active segments with a capacitance and ionic currents. In the MCB condition these two segments behaved as fully isolated elements.

of the unmyelinated cell body on the spike propagation. The need for the unmyelinated pre-somatic region is also explained in that study, showing that this region is needed for the action potential to bridge the large capacitor formed by the unmyelinated cell body. It forms a safety factor to ensure the propagation of the AP along the nerve fiber. Similar to Rattay et al. (2001b), both on the soma and on the pre-somatic region 4 myelin wraps are included to enable AP propagation across the cell body. This thinly myelinated situation is called unmyelinated for clarity and in accordance with the description and naming in Rattay et al. (2001b). To model the cell body and the presomatic region, nodes of Ranvier, were added to these segments with corresponding diameters. The myelin wraps (N) can be seen as a series of membranes, each with the same capacitance and conductance. Using the scale factor $\frac{1}{1+N}$ the capacitance and conductance could be calculated for a certain number of myelin wraps (with 4 myelin layers this leads to $C_m = 3.52pF$ and $G_L = 0.75n\Omega^{-1}$ for the presomatic region and $C_m = 5.28pF$ and $G_L = 1.13n\Omega^{-1}$ for the cell body). The current strengths of the ionic currents were however reduced by an extra factor 30 compared to the nodes of Ranvier (inset Fig. 8.2). To investigate to what extent the UMCB contributes to the observed differences between eCAP recordings between animals and humans, also a myelinated cell body (MCB) condition was used, where the cell body and the pre-somatic region are fully myelinated. As in the model of Rattay et al. (2001b) the number of inter-nodes

in the peripheral process for both the MCB and UMCB condition has been increased from 4 to 6 to deal with the fact that the trajectory from the tip of the fiber to the cell body is much larger in humans than in guinea pigs. However, although more inter-nodal segments are used in the peripheral process, the position of the cell bodies in the spiral ganglion is in accordance with histological data like in our previous studies with a human cochlear geometry (Frijns et al., 2001). To fit the peripheral process into the anatomically correct position its length is scaled to match the trajectory from the spiral ganglion to the organ of Corti. The nodes of Ranvier and the unmyelinated segments include a membrane capacitance, active sodium and potassium ionic channels and a passive leak conductance (Fig. 8.2, inset). The equations governing the kinetics of this so-called generalized Schwarz-Eikhof-Frijns (GSEF) auditory nerve fiber model are described in detail elsewhere (Frijns et al., 1994; Frijns et al., 1995; Frijns et al., 2000a) and will not be repeated here.

8.2.2 The backward problem: calculation of the compound action potential

Essentially, an AP is a depolarization of the cell membrane at the nodes of Ranvier, which propagates along the nerve fiber. The processes of depolarization and repolarization are characterized by current flowing into and out of the fiber through the nodal membrane. In fact, recording the eCAP is the simultaneous registration at a single recording electrode of the potentials induced by these nodal currents. In the computational model this concept of eCAP generation is applied, while taking into account four different current components in each modeled node of Ranvier (inset of Fig. 8.2) viz. the current $I_k^C(t)$ through the membrane capacitance, $I_k^{Na}(t)$ and $I_k^K(t)$ through the sodium and potassium ionic channels and $I_k^L(t)$ through the leak conductance. This means that the contribution of a single node of Ranvier k is given by the net current $I_{f,k}(t)$ leaving the fiber f through this node as a function of time t:

$$I_{f,k}(t) = -(I_{f,k}^C(t) + I_{f,k}^{Na}(t) + I_{f,k}^K(t) + I_{f,k}^L(t)) \tag{8.2}$$

The potential at the recording electrode as induced by each nodal current $I_{f,k}(t)$ can be calculated by application of the reciprocity theorem: the same transfer resistance that exists between a stimulating electrode and a particular node of Ranvier gives the relationship between a current through that node of Ranvier and the electrode when used to record the eCAP:

$$V_{f,k}^{rec}(t) = R_{f,k}^{rec} I_{f,k}(t), \tag{8.3}$$

where $V_{f,k}^{rec}(t)$ is the potential on the recording electrode rec induced by $I_{f,k}(t)$ and R^{rec} is the corresponding resistance matrix (standard electrode #1 is used). To obtain the single fiber action potentials of each fiber $\text{SFAP}_f^{rec}(t)$ on the recording electrode the contributions of all the nodes of Ranvier of a fiber are combined

$$\text{SFAP}_f^{rec}(t) = \sum_k V_{f,k}^{rec}(t). \tag{8.4}$$

Finally, all SFAPs must be combined to create the potential $V^{rec,total}(t)$ as would be measured at a recording electrode as a function of time:

$$V^{rec,total}(t) = \sum_f \text{SFAP}_f^{rec}(t). \tag{8.5}$$

The above summation has to be performed at each moment in time where the eCAP has to be calculated. Since each fiber in the simulation represents 100 actual fibers, $V^{rec,total}(t)$ has to be multiplied by this factor for comparison with actual measurements. All eCAP responses in this paper were sampled at 10μs intervals, although the integration of equations governing the individual nerve fibers took place with a fourth order Runge-Kutta method with adaptive step size control in order to ensure numerical accuracy (Frijns and ten Kate, 1994). Therefore, fourth order polynomial interpolation was used to obtain the nodal current strengths in all the fibers at the predefined, evenly spaced time intervals.

8.2.3 The use of an artifact rejection scheme

Although the capacitance at the level of the electrode to fluid interface (the main source of stimulus artifacts in actual eCAP recordings) is not incorporated in the present model, there turned out to be a considerable stimulus artifact in the simulated eCAPs. This artifact is caused by the membrane capacitance of the nodes of Ranvier and especially in the unmyelinated cell body. This artifact is up to an order of magnitude larger than the neural response and can obscure or disfigure it just as is the case in actual recordings. We concluded that the simulations too would benefit from an artifact rejection scheme.

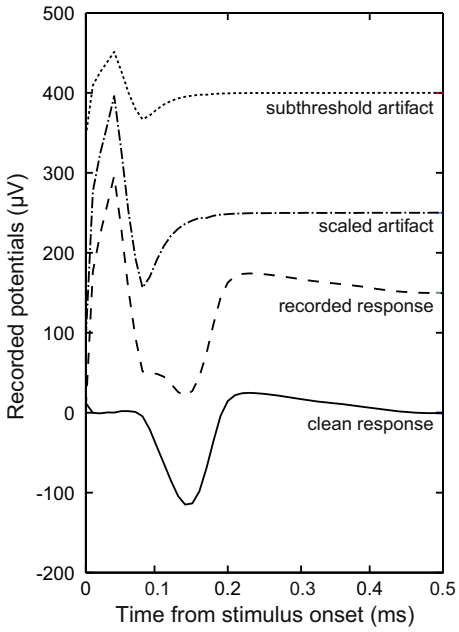

Figure 8.3: Visualization of the scaled artifact method. The response of a subthreshold stimulation is recorded (dotted line) and scaled (dash dotted line) to fit the amplitude of the artifact in the supra-threshold recording (dashed line). By subtracting the scaled artifact from the recorded response, a response without artifact is obtained (solid line)

From experimental studies three artifact rejection schemes are known: alternating polarity, forward masking (MP3) and scaled artifact; all three are based on different neural properties. All three methods have been tested with the model, and lead to the conclusion that the clinical drawbacks of each of the different methods (Klop et al., 2004) also apply to the model situation. The alternating polarity paradigm uses the fact that the polarity of the CAP is equal for anodic and cathodic stimuli while the artifact polarity is linked to that of the stimulus. However, there are fundamental differences in the neural response to cathodic and anodic stimulation, making this paradigm less appropriate for a theoretical study like the present one. The forward masking paradigm uses the refractory period of the nerve fibers to create a stimulus artifact without an eCAP which is then used to cancel the artifact of the intended eCAP response. For several reasons this paradigm, which is clinically the most widely

used, is also not optimal for the present study. First, the timing of the pulses in this paradigm is dictated by the refractory behavior of the neural elements. In the model, this refractory behavior has not been fully evaluated yet and is subject of ongoing research in our laboratory. Second, the calculation of the response to a double pulse takes 4-5 times more time than determining the response to a single pulse. Such an increase in calculation time is a considerable drawback of this method. Therefore, the scaled artifact paradigm is used throughout this study. It uses the artifact from a sub-threshold stimulus, scaled to fit the artifact of the response under study, which is then subtracted from the calculated eCAP to remove the artifact (Fig. 8.3). Clinically, the validity of this method is limited by the intrinsic non-linearity of the electrode to fluid interface, the uncertainty that the artifact is really without a neural response and the fact that the noise in the recording of the artifact is scaled with the artifact. In the present model the electrode to tissue interface is not incorporated, which eliminates the major flaws of the method. In addition, for the model situation, recording noise and unknown fiber excitation do not exist. The calculated SFAPs change less then 1% when the step size of the fiber models is reduced by a factor 10, indicating sufficient numerical accuracy.

8.3 Results

The most detailed presentation of the outcome of the forward problem is the so-called excitation profile as shown in Fig. 8.4. Such a plot depicts which nerve fibers get excited at various stimulus levels. The location of the initial excitation (peripheral process, cell body or modiolar axon) is indicated by the degree of shading. Fig. 8.4^A shows such an excitation profile for the standard conditions as defined in section 8.2, as calculated with the old, guinea pig based, fiber (GSEF) used in previous human model studies (Frijns et al., 2001; Frijns and Briaire, 1999). Fig. 8.4^B shows the same result for the present human nerve fiber morphology (UMCB condition). It is clear from these figures that the shapes of the profiles are very similar. The main differences are an upward shift in threshold for the UMCB fiber, and a change in excitation site, especially along the edges of the excitation area where the fibers are stimulated just above threshold level. In the GSEF fiber morphology the peripheral process is excited at threshold level, where it is the central axon in the human fibers. The excitation profile for the MCB condition is not presented, since it resembles the presented plots very closely: the thresholds for the MCB and UMCB fibers are almost identical, while the initial excitation

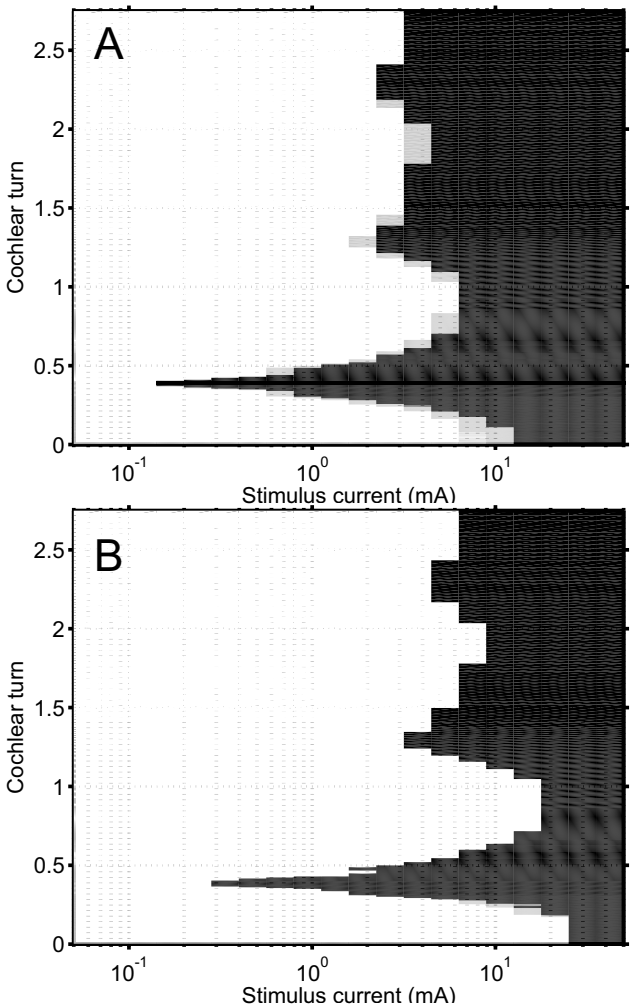

*Figure 8.4: Excitation profile for the nerve fiber used in previous studies (**A**) and for the UMCB condition (**B**). In these profiles is depicted which nerve fibers get excited for a certain current strength. The location where the initial excitation occurs is indicated by the degree of shading (light gray: peripheral process and black the modiolar axon). For this setting there is no initial excitation on the cell body and the surrounding nodes.*

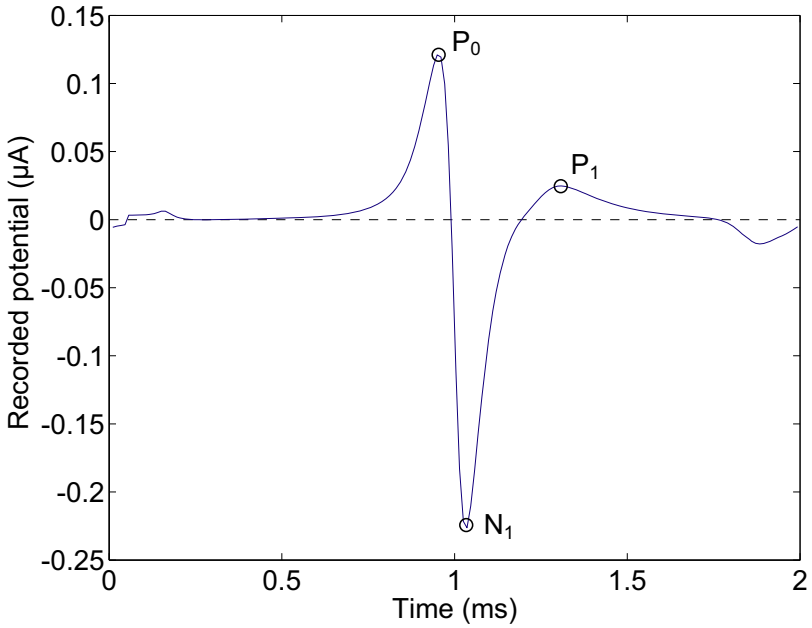

Figure 8.5: Single fiber action potential (SFAP) from a straight uniform nerve fiber (with 100 segments of 350 μm, like the central axon of the used auditory nerve fiber) in a infinite homogeneous medium. The recording electrode is placed 17.5 mm from the tip of the nerve fiber and 0.6 mm from the fiber axis.

site for the MCB tends to shift to the cell body for the fibers along the edges of the excitation area. These observations indicate that previously published conclusions based on excitation profiles computed with the GSEF fiber are still in line with the present results.

As described in the previous section, obtaining the eCAP with the model involves a sequence of calculation steps. First, the currents from all the nodes of Ranvier have to be calculated. Next, their contribution on the potential at the recording electrode has to be computed, yielding the SFAPs for each fiber. Finally, all SFAP contributions must be superimposed to get the final eCAP, Eq. (8.5). As an initial validation of the principle of calculating the eCAP in the way described above, the procedure was tested in a single uniform nerve fiber in an infinite, homogeneous medium. The segments of this uniform nerve fiber are the same as the axonal part of the MCB and UMCB auditory nerve fiber (with an inter-nodal length of 350 μm). According to the theories developed for

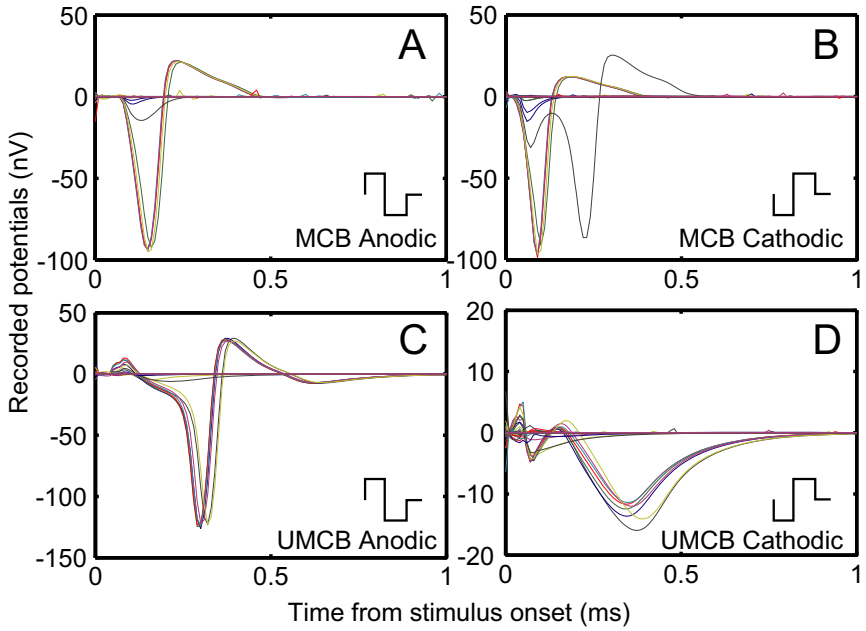

*Figure 8.6: All the SFAPs as recorded from the most apical contact at approximately 1.5 turns insertion depth induced by a current, 6 dB above threshold for the (**A**) MCB anodic-first, (**B**) MCB cathodic-first, (**C**) UMCB anodic-first and (**D**) UMCB cathodic-first condition.*

EMG recordings (Schoonhoven and Stegeman, 1991) an asymmetric triphasic SFAP is expected for relatively small recording distances as used in this test. The simulated SFAP is plotted in Fig. 8.5. When the AP gets close to the recording electrode a sharp positive peak (P_O) becomes apparent followed by a large negative peak (N_1). When the AP finally propagates away from the recording electrode a more shallow positive P_1 peak is induced. Therefore, the test case behaves in line with the theoretical expectations. From this and similar experiments we concluded that the algorithm for the backward problem is conceptually correct.

In Fig. 8.6 the full volume conduction and neural model with the MCB and UMCB auditory fiber morphology were used to calculate SFAPs for anodic-first and cathodic-first biphasic current pulses. These calculations were made for a stimulation level that was 6 dB above the threshold (the current strength at which the first modeled fiber is excited) for the standard condition of the model. For the anodic-first MCB condition (Fig. 8.6^A) the first positive peak

P_0 is not discernible in these responses, as can be expected from the fact that the AP cannot really propagate towards the recording electrode. This is the consequence of the fact that the excitation site is close to the recording electrode. The N_1 and P_1 peaks are clearly visible, with absolute latencies of N_1 and P_1, around 0.15 ms and 0.24 ms after stimulus onset respectively. In Fig. 8.6^B the SFAPs for a cathodic-first stimulus are plotted. Again, no P_0 peak is observed, but the majority of the responses have shorter latencies with N_1 at 0.1 ms, i.e., very close to the artifact, and P_1 at approximately 0.18 ms. This means that these latencies are 50-60 μs shorter then the ones found for the anodic-first condition. There is one SFAP with a longer latency. This originates from the nerve fiber at the edge of the excitation area. This fiber is stimulated just above threshold level and it takes some time before the AP starts propagating.

To clarify the mechanism underlying these latency differences between cathodic- and anodic-first stimulation, the propagation of the AP along a fiber at the center of the excitation area was analyzed in so-called AP-plots (Figs. 8.7^{A,B}). In these plots the deviation (V_k) of the transmembrane potential from the resting membrane potential is plotted for all nodes of Ranvier as a function of their position along the nerve fiber. The tip of the peripheral process is located at 0 mm, the cell body at approximately 2 mm. For the fiber under study the stimulating electrode is located near the cell body, i.e., at approximately 2 mm along the fiber. The different curves in Fig. 8.7 represent V_k at 10μs intervals:

$$V_k = V_i - V_e - V_r \tag{8.6}$$

with V_i the internal potential, V_e the external potential and V_r the resting membrane potential. The first curve is taken at stimulus onset, i.e. at the start of the first stimulus phase. For clarity a thick line has been added in each of the two stimulus phases. For instance, during an anodic stimulus (first three lines in Fig. 8.7^A), the external potential is elevated ($V_e \uparrow$), with a much lower internal potential, resulting (Eq. (8.6)) in a negative V_k at the stimulus site. At the same time, because of the potential difference, current is flowing into the nerve fiber, thereby increasing the internal potential at the stimulus site. This current is than transported along the nerve fiber, increasing V_i at the nodes surrounding the stimulus site. At these nodes V_e is only slightly elevated due to the stimulus, leading to a net raise of the transmembrane potential V_k on both sides of the stimulation site (visible in the dashed line of Fig. 8.7^A). However,

the nerve fiber only starts reacting after the second stimulus phase, which induces a positive V_k at the excitation node. After the stimulus, this positive V_k is maintained at the excitation node and the region of positive V_k's even broadens due to the active processes in the nerve fiber. This process continues until 50 μs after the end of the stimulus. The peak then splits in two, and two APs start propagating in opposite directions. For clarity the propagating APs have been indicated with gray bars in the plots.

The AP-plot for the cathodic-first MCB condition, where SFAPs with a short latency were found (Fig. 8.6^B), is shown in Fig. 8.7^B. The fiber is stimulated most in the nodes of the central axon next to the cell body at 2.1 mm from the tip of the fiber. This excitation site is due to the use of a peri-modiolar electrode array in this study. The fibers on the edge of the excitation area are excited in the peripheral process, as can be seen in the excitation plots. The first negative stimulus phase induces a positive V_k, leading to a depolarization. Thus the fiber reacts immediately on the first negative stimulus phase and two APs occur, one moving antidromically toward the organ of Corti and one (orthodromic) along the central axon. The second stimulus phase helps to split up the two APs. The difference in AP arrival at the central end of the modeled fiber is approximately 70 μs, where the cathodic-first situation is the earlier one. The hypothesis that the fiber is initiated during the cathodic phase of the stimulus in both the anodic- and cathodic-first stimulus conditions can not account for this large delay, since the phase duration is as short as 37.5 μs. In fact, the initiation process is different, and this adds a major contribution to the delay, which is also reflected in the latency difference between the SFAPs from the anodic- and cathodic-first stimulation (Fig. 8.6^A vs. 8.6^B).

The SFAP responses from UMCB condition of the fiber morphology, as shown in Fig. 8.6^{C,D}, have completely different characteristics compared to the MCB condition. The anodic-first stimulus leads to a delayed response with the N_1 peak around the 0.3 ms, followed by a P_1 peak at 0.45 ms. The cathodic-first response (Fig. 8.6^D) shows only a very broad and shallow N_1 peak. Again, the corresponding AP-plots (sub-figures 8.7^{C,D}) will be used to get a better understanding of these wave forms. For the anodic-first stimulus the downward (orthodromic) propagating AP in the UMCB condition (Fig. 8.7^C) behaves similar to the orthodromic AP in the MCB condition (Fig. 8.7^A). On the other hand, the AP propagating upward (antidromic) to the peripheral process is delayed by the cell body. The timing of the delayed SFAP shown in Fig. 8.6^C fits best to this AP, moving to the tip of the fiber. To get an indication of the delay induced by the cell body the AP-plot of a fiber excited at the peripheral process by an apical lateral wall electrode (contact #1) at threshold

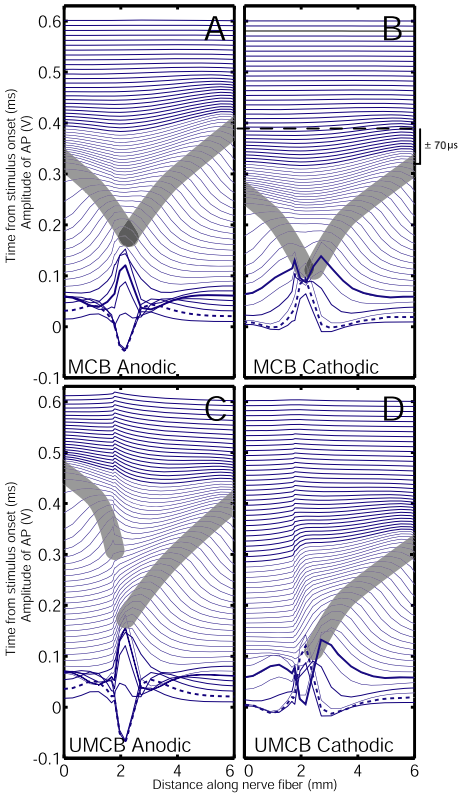

*Figure 8.7: In these AP-plots the intracellular potential of a fiber at the center of the excitation area is plotted as a function of the distance along the nerve fiber from peripheral process (0mm) to the cell body at approximately 2 mm and further along central axon ($>$ 2.1 mm). The different lines represent different time steps of 10μs each, with the bottom line t=0. A dashed and a solid line have been added at the end of respectively the first and second phase of the stimulus. The gray bars indicate the trajectory of the AP along the nerve fiber. The excitation is induced by a current 6 dB above threshold in the (**A**) MCB anodic-first, (**B**) MCB cathodic-first, (**C**) UMCB anodic-first and (**D**) UMCB cathodic-first condition.*

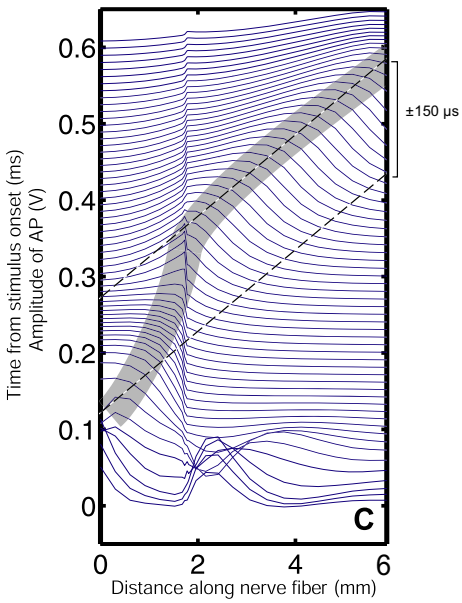

Figure 8.8: The AP-plot for a nerve fiber excited at the peripheral process by an apical contact along the medial wall. The gray bar indicates the trajectory of the AP along the nerve fiber. By extrapolating the trajectory of the AP it is estimated that the delay induced by the unmyelinated cell body is approximately 150 μs.

level is shown in Fig. 8.8. Without obstructions the AP propagates with a constant velocity, in other words along a straight line. This is clearly the case for distances above 2 mm along the nerve fiber. By extrapolating the trajectory of the AP in the peripheral process it is possible to get an indication of the delay induced. By measuring the vertical distance between the actual trajectory and the extrapolated trajectory, a somatic delay of approximately 150 μs is found, which roughly corresponds with the delay found in the calculated SFAPs.

In the case of a cathodic-first stimulus (Fig.8.7^D) the second AP, propagating to the dendrite is not able to cross the cell body, and the potential slowly decreases back to the resting state (Fig. 8.6^D). The first cathodic phase depolarizes the nerve fiber and two APs are initiated as usually. The antidromic AP is propagating very slowly through the cell body. The second positive phase has a negative effect on the depolarization of the unmyelinated elements and leaves a charge on the capacitors, cancelling the sodium influx. In addition, contrary to the situation with an orthodromic AP crossing the cell body, there

is also no pre-somatic region helping the AP to cross the unmyelinated cell body in antidromic direction. This combination makes that the nodes in the peripheral process are not depolarized and the AP is aborted.

All SFAPs described above were calculated at a current strength of 6dB above threshold. Clinically the NRT or NRI capabilities of the implants are mostly used to record IO-curves, which in turn are used to determine the corresponding thresholds. The same experiment has been simulated with the computer model. Clinically, the use of anodic-first pulses is preferable for eCAP measurements because of their slightly longer latencies compared to the cathodic-first pulses (Klop et al., 2004), reducing the interference of the stimulus artifact. Therefore, also for this experiment anodic-first biphasic pulses have been used to calculate five eCAPs at different current strengths with 3 dB intensity steps. In Fig. 8.9 these eCAPs have been plotted for the MCB condition. The bottom line was calculated for the lowest current strength, and shows a small eCAP consisting out of an N_1 and P_1 peak. When the current levels rise, the latency of both peaks is slightly reduced and the peaks become larger. At the highest levels the P_1 peak becomes less pronounced and even the amplitude of the N_1 peak starts to reduce. At the same time a very sharp P_0 peak shows up. The corresponding IO-curve, which depicts the N_1P_1 amplitude, is plotted in Fig. 8.10 together with the same curve, now based on the number of excited nerve fibers. For the lower current strengths both curves are very similar. At higher current levels, however, the calculated N_1P_1 amplitude decreases while the number of fibers that get excited keeps increasing monotonously. The same phenomenon can be seen in the calculated UMCB responses (not shown), where the N_1P_1 amplitude starts to reduce at even lower current strengths. In both cases the reduction of the N_1P_1 amplitude is accompanied by a growing P_0 peak. To get insight in the causes of this phenomenon, the distributions of the MCB SFAPs contributing to the eCAP induced by an anodic-first stimulus have been plotted in Fig. 8.11. The amplitude is color-coded with red designating a positive amplitude and blue a negative one, while the SFAPs are ordered for fibers from base to apex along the vertical axis. Horizontally the time has been plotted. For low stimulation levels (Figs. 8.11^{A,B,C}) the single fiber contributions are very homogeneous, first a blue negative part (N_1) followed by a red positive potential (P_1). When the current strength increases, however (Fig. 8.11^{D,E}), the of the response of the center part changes, and adds a highly different contribution to the eCAP, which leads to the P_0 peak. Similar observations were done for cathodic-first and anodic-first stimulation of the UMCB nerve fibers (not plotted here), but this effect was not detected at all in the cathodic-first stimulation of MCB nerve fibers.

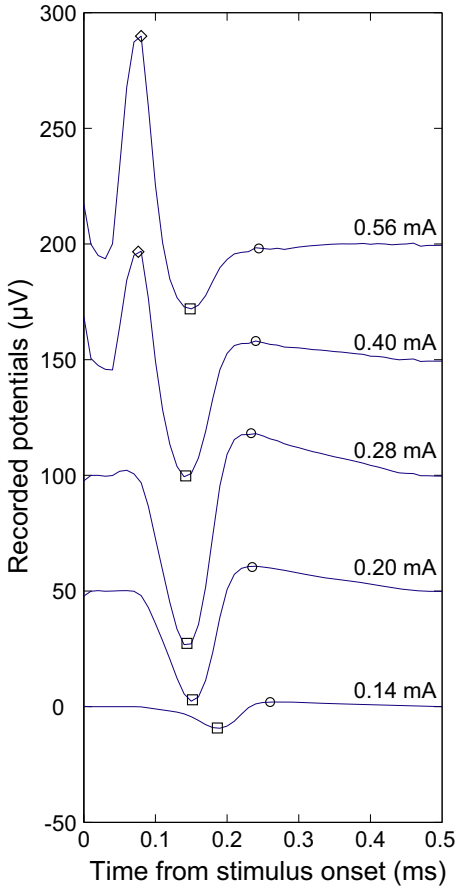

Figure 8.9: The calculated eCAP responses for the MCB condition, as induced by anodic-first biphasic current pulses for five current strengths. The N_1 and P_1 peaks are indicated by squares and circles, respectively. The P_0 visible at higher current strengths are indicated by a diamond.

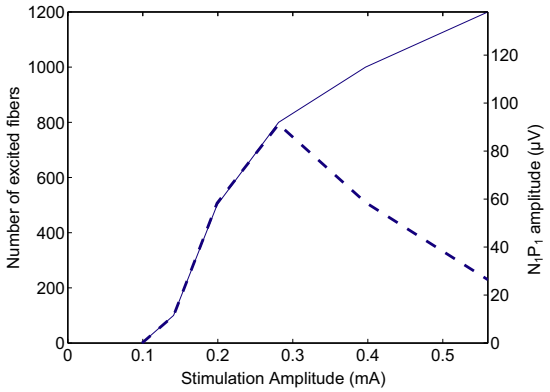

Figure 8.10: The response amplitude (N_1-P_1 difference) (dashed line) and the number of excited nerve fibers against the current strength (solid line) as a function of the stimulation strengths.

The explanation why the fibers in the center of the excitation area have a different contribution to the eCAP at higher stimulus levels, becomes clear from Fig. 8.12. In Fig. 8.12^A the AP plot of an MCB fiber (anodic-first stimulation) at the center of the excitation area is plotted. Due to the large stimulation currents used (0.40 mA, cf. Figs. 8.9 and 8.11^D), the orthodromic AP starts further away from the site where the current is injected, while the antidromic AP is indiscernible. The propagating orthodromic AP is already too far away along the central axon to have any significant contributions to the SFAP as recorded on contact #1. The resulting SFAP is characterised by a large P_0 peak followed by a shallow N_1 peak. The nerve fibers at the border of the excitation area have a very similar AP propagation (Fig. 8.12^B) as the fibers at the center when lower current strengths are used (Fig. 8.7^A). In summary the P_0 peak only occurs at the higher current strengths and originates from the fiber population at the center of the excitation area for both the MCB and UMCB condition.

8.4 Discussion

In this study the mechanisms behind the eCAP are investigated with a computational model. The model consists of a realistic three-dimensional cochlea

model combined with an active, non-linear nerve fiber model. To be able to calculate the eCAP properly, the model had to be extended to allow for recording of the currents generated in the nerve fiber model through the volume conduction model of the cochlea. The generated currents and the recording algorithm used in a long and homogeneous nerve fiber produce SFAPs (Fig. 8.5) with a shape very comparable with more fundamental predictions and actual measurements (Schoonhoven and Stegeman, 1991). From this elementary experiment we conclude that the described algorithm for SFAP calculation from an active nerve fiber model is functioning correctly.

The peak latencies found in the full model, however, do not match the human situation (Frijns et al., 2002; Abbas et al., 1999). The latencies are short, and fit much closer to recorded eCAPs from the guinea pig (Klop et al., 2004). The changes made to the morphology, i.e., adding more segments in the peripheral process, increasing the size of the cell body and removing the myelin layers from the cell body and pre-somatic region, as was indicated by the study of Rattay et al. (2001a), did not yield more accurate eCAPs or SFAPs. However, the changes did result in an upward threshold shift because the capacitance of the cell body worked as a drain for the stimulating current. The main effect ascribed to the unmyelinated cell body by Rattay et al. (2001a), the somatic delay in AP propagation, does occur with the UMCB morphology as can be seen clearly from Fig. 8.8, where is shown that the cell body in our UMCB model causes a delay of approximately 150 μs.

It seems that, although the morphology has been adapted to the human situation, the shape of the calculated eCAP and thus also the shape of the AP resembles more closely the animal situation on which the nodal kinetics are based (Schwarz and Eikhof, 1987). The amplitude of the calculated response is also smaller (factor 2-4) then the recorded human eCAP response. The various changes to the morphology lead to specific effects in the behavior of especially the UMCB fiber, such as the somatic delay described by Rattay et al. (2001a), but do not lead to an accurate human eCAP response. This somatic delay induces an increased overall latency of the SFAP responses as plotted in Fig. 8.6^C for the UMCB fiber, but the inter-peak interval invariably remains too short. Current investigation at our center focuses on implementing human kinetics (Wesselink et al., 1999) into our nerve fiber model, which appears to influence the shape and propagation speed of the AP and may lead to a more realistic eCAP wave form.

In spite of the fact that the delayed SFAPs as shown for the UMCB condition with anodic first stimulation (Fig. 8.6^C) correlates with the above mentioned

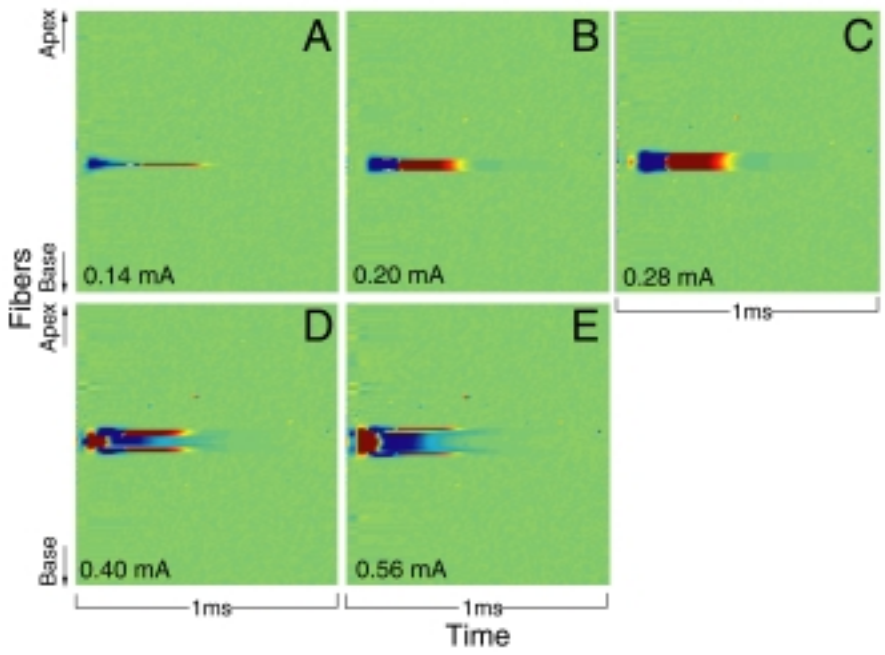

Figure 8.11: The SFAPs for the nerve fibers ordered from base to apex as a function of the time. The amplitude is color-coded with blue a negative potential and red a positive potential. The SFAP-distribution is plotted for the same five different anodic-first biphasic current steps in the MCB condition used to get the IO-curve of Fig. 8.10.

somatic delay, the excitation of the orthodromic AP takes place directly in the central axon, and this AP can thus propagate to the brain without passing the delaying cell-body. The same observation holds for the cathodic-first stimulation (Fig. 8.6^D). In this situation a very normal AP propagates along the central axon as can be seen from the AP-plot (Fig. 8.7^D). Nevertheless a distorted eCAP wave form is recorded (Fig. 8.6^D). Looking closely to the two AP-plots (Fig.s 8.7^{C,D}) one notices that for the anodic-first situation the antidromic AP does have a delay corresponding to the delayed SFAP response, while the antidromic AP is abortive in the case of cathodic-first stimulation. Such a terminated AP could be responsible for the small negative potential seen in the SFAP plot. From these observations one can deduce that the current emitted by the unmyelinated cell body dominates the response in the UMCB condition. The AP trajectory plotted in Fig. 8.7^D might closely resemble the AP plot for degenerated nerve fibers (i.e., without peripheral processes). This could explain the absence of NRI or NRT responses in some patients with neural degeneration while they have very normal auditory sensations and good performance. A recent paper about antidromic action potentials (Miller et al., 2004) already indicated that two APs are present and that the initial positive peak in the eCAP originates from antidromic APs originating from a relatively central site of excitation. This corresponds in part with our finding that the dendrite is responsible for the generation of the P_0 peak. The presence of the P_0 peak at higher current strengths, which originates from the central part of the excitation area, is subject of ongoing model studies. That study indicates that the state of neural degeneration of the fibers has a big influence on the presence of the P_0 peak.

The dominance of the response by the current from the cell body could be reduced if a leaking cable model were used. In that way the whole fiber would emit more current and the SFAP would give a more balanced view on the behaviour of the fiber as a whole. With the current model (Frijns and ten Kate, 1994; Frijns et al., 1994; Frijns et al., 1995), based on the work of Schwarz and Eikhof (1987), it is not possible to add these leaking compartments while maintaining realistic AP conditions without increasing the nodal current densities. This problem was solved by Rattay, who uses a Hodgkin and Huxley (1952) based model, by increasing the sodium, potassium and leakage conductance by a arbitrary factor 10, therby assuming higher channel densities in the nodes of Ranvier. We hope to be able to add the leaking compartments and a conduction layer between the myelin and the central axon (Halter and Clark, 1991) with the new human kinetics.

Although the morphology of the MCB condition is more like the fiber found in

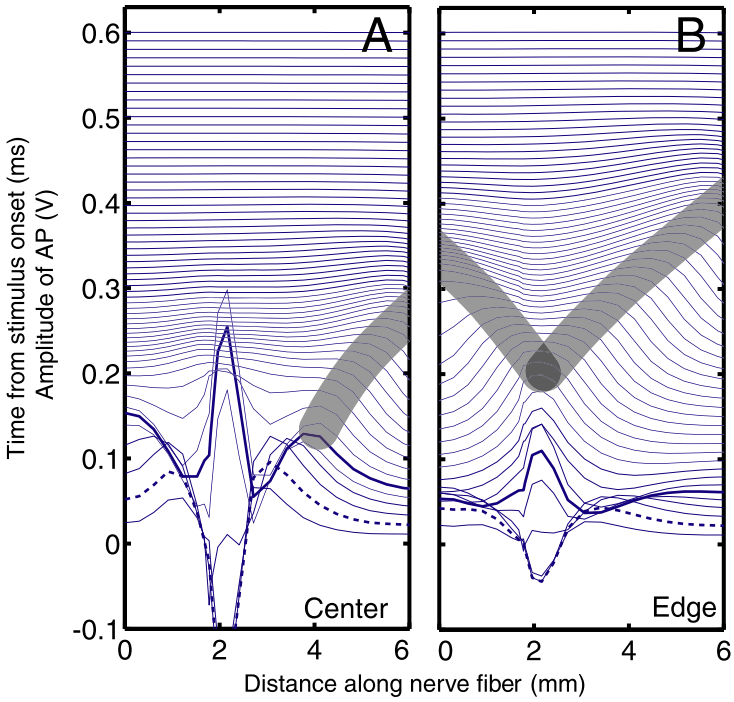

*Figure 8.12: The AP-plots for (**A**) a fiber at the center of the excitation area and (**B**) a fiber at the edge of the excitation area for a large stimulus current (12 dB above threshold) where the center part of the fibers does not give a contribution to the eCAP response.*

animal experiments, it is still a valuable tool to get understanding of the processes occurring during electrical stimulation and their effect on eCAP recordings. For example, an influence of stimulus polarity on the in vivo recorded eCAP was observed (i.e., anodic-first stimulation resulted in a response, which was delayed approximately 60 μs longer than that with cathodic-first stimulation). This has been a topic of recent studies (Klop et al., 2004; Miller et al., 1998), especially since there are direct consequences for using the alternating polarity artifact rejection scheme to measure the eCAP. In our model we find a very similar result (Fig. 8.6^{A,B}) with a delay of 50-60 μs. From the analysis of the AP-plots (Fig. 8.7^{A,B}) it becomes clear that the initiation process of the AP explains the latency shift. The anodic-first stimulus excites the nerve fiber at one place close to the electrode contact, while the cathodic-first stimulus induces two APs just next to the stimulation site. This behavior is similar to that

seen in responses to mono-phasic stimulation with the polarity of the second stimulus phase.

From these AP-plots it is also clear that in most cases for a peri-modiolar electrode array there are two simultaneous APs, one orthodromic, and one antidromic. Both can induce a biphasic response on a recording electrode. As mentioned above, for the UMCB condition the presented responses are actually dominated by the antidromically propagating AP. With this in mind it can be expected that the exact placement of the recording electrode is also of importance. In this study the most apical electrode has been used as the recording contact, probably giving a preference to the antidromic AP because of the proximity and the perpendicular orientation of the peripheral process, while the central axon is directed away from the recording contact. It is conceivible that the ortho- and antidromic APs have a varying relative contribution to the eCAP recorded at the various recording contacts along the array when a scanning method is used to measure spatial selectivity (Frijns et al., 2002; Abbas and Brown, 2000). Apical recording contacts will preferably register the upward moving AP where the basal recording electrodes will mainly see the downward propagating signal. The situation as plotted in Fig. 8.8 with only one AP moving along the fiber is only found in lateral wall electrodes or more apical contacts where the initial excitation occurs in the peripheral process .

It has been indicated above that the currents of the cell body and the surrounding nodes dominate the overall eCAP response. This is deduced from the fact that the latencies of the calculated eCAPs match with the propagation of the antidromic AP passing through these segments. Differentiating between the contributions to the SFAP of various nodes of a nerve fiber is very difficult, because the potentials induced by a single node on the recording contact are some magnitudes larger than the final SFAP. The SFAP is defined by the very small differences between the contributions of the individual nodes. Blocking some nodes for instance from contributing to the SFAP, in an attempt to differentiate between the various segments, disrupts this balance and makes the outcome useless. This makes it impossible to exactly indicate what part of the fiber, or AP trajectory is responsible for a certain change in the recorded SFAP.

The nerve fibers turned out to give other SFAPs at high (Fig. 8.11^C) than at low (Fig. 8.11^D) current strengths. This is also reflected in the AP plot (Fig. 8.12^A vs. 8.12^B). At high stimulation levels the AP is initiated further along the nerve fiber, causing it not to contribute to the N_1P_1 complex of the eCAP. Such high currents induce a mono-phasic neural potential on the recording contact. The nerve fibers at the edges of the excitation area only receive a current

just above threshold due to the distance from the stimulating electrode, and they will produce normal SFAPs. Their contribution to the eCAP is similar to the one seen close to the stimulating contact for low current strengths. The consequence of this behavior for clinical practice is that during eCAP measurements the slope of the IO-curve is shallower than that predicted by the increase of the number of excited nerve fibers. Moreover, the amplitude of the response can saturate or even decrease for larger current strengths. The same phenomenon has also been reported in cat experiments by Miller et al. (1998) (their Fig. 8) who found a decrease in the eCAP amplitude-level function at higher current strengths. He observes, that saturation of the IO-curve does not automatically indicated that all fibers are active and contributing to the recorded eCAP response.

The mono-phasic contribution of fibers from the center of the excitation area resembles a P_0 peak as can be seen clearly in Fig. 8.9. Theoretical models of neural excitation (Schoonhoven and Stegeman, 1991) also predict the presence of such a peak, but then it originates from the AP approaching the recording site. This mechanism was also demonstrated with the current model using a homogeneous nerve fiber (Fig. 8.5). In an actual recording it would not be possible to discriminate between the two sources of the P_0 peak. One would only record its presence. By investigating the individual contribution of the nerve fibers and the trajectories of the APs it becomes clear that the P_0 peak from our model simulations is not the effect of an AP propagating toward the recording electrode but of the initiation of an orthodromic AP further along the nerve fiber, deep in the modiolus.

This necessarily means, that for electrical stimulation, the unitary response theory (i.e., where every fiber contributes the same amount to the whole nerve response) is not valid. The fibers from the center of the excitation area give a different, mono-phasic, contribution where the edges give a bi-phasic response with a typical N_1P_1 pattern. For an electrode, located near the lateral wall, the model predicts excitation in the peripheral processes. In this situation the somatic delay will be added as an extra delay to the AP propagation. This would result in a further delayed SFAP, which also does not fit into the unitary response concept. This variation of the SFAP contributions is less when a recording contact further away from the cochlea, for instance along the auditory nerve trunk is used, like in some animal experiments (Miller et al., 2003; Houben et al., 2000). These remote recoding sites are probably better then intracochlear electrodes to study neural recruitment and latency shifts as observed by the brain.

The model extension to allow for eCAP response calculations allows us to study the fundamental principles underlying the eCAP response. The newly introduced fiber morphology with an unmyelinated cell body and pre-somatic region, functions correctly for studies of excitation and propagation of the AP. The dominance of the cell body on the simulated eCAP should however be further investigated and validated. Future studies must incorporate a more realistic human fiber model, which produces more correct latencies. The simulations give insight in the differences between the SFAPs and indicate that at high current strengths the center part of the excitation area does not contribute to the N_1P_1 complex in recorded eCAP responses but gives rise to a P_0 peak. They also explain a negative slope of IO-curves, in spite of monotonously increasing numbers of excited fibers.

8.5 Acknowledgement

This research was financially supported by grants from the Hoogenboom-Beck-Fund and the Heinsius Houbolt Fund. We thank Prof. Dr. J.J. Grote, former head of our department, for his continuing support.